

# Early-mid Miocene erosion rates inferred from pre-Dead Sea rift Hazeva River fluvial chert pebbles using cosmogenic $^{21}\text{Ne}$

Michal Ben-Israel<sup>1</sup>, Ari Matmon<sup>1</sup>, Alan J. Hidy<sup>2</sup>, Yoav Avni<sup>3</sup>, Greg Balco<sup>4</sup>

<sup>1</sup>*The Institute of Earth Sciences, Hebrew University of Jerusalem, Jerusalem, 91904, Israel*

5 <sup>2</sup>*Center for Accelerator Mass Spectrometry, Lawrence Livermore National Laboratory, Livermore, CA 94550, USA*

<sup>3</sup>*Geological Survey of Israel, Yesha'yahu Leibowitz 32, Jerusalem, 96921 Israel*

<sup>4</sup>*Berkeley Geochronology Center, Berkeley, California 94709, USA*

*Correspondence to:* Michal Ben-Israel (michal.benisrael@mail.huji.ac.il)

**Abstract.** In this work, we utilize a novel application of cosmogenic  $^{21}\text{Ne}$  measurements in chert  
10 to compare exposure times measured in eroding surfaces in the Jordanian Central Plateau with  
exposure times from chert pebbles transported by the Miocene Hazeva River. The Miocene Hazeva  
River was a large fluvial system (estimated catchment size  $>100,000 \text{ km}^2$ ) that drained the Arabian  
Plateau and Sinai Peninsula into the Mediterranean Sea during the early-mid Miocene. It was  
established after the rifting of the Red Sea uplifted the Arabian Plateau during the Oligocene.  
15 Following late Miocene to early Pliocene subsidence along the Dead Sea Rift, the Hazeva drainage  
system was abandoned and dissected, resulting in new drainage divides on either side of the rift.  
We find that modern erosion rates derived from cosmogenic  $^{21}\text{Ne}$ ,  $^{26}\text{Al}$ , and  $^{10}\text{Be}$  in exposed *in situ*  
chert nodules to be extremely slow, between 2-4 mm/kyr. Comparison between modern and  
paleo-erosion rates, measured in chert pebbles, is not straightforward, as cosmogenic  $^{21}\text{Ne}$  was  
20 acquired partly during bedrock erosion and partly during transport of these pebbles in the Hazeva  
River. However, even with bedrock erosion and maintained transport along this big river,  $^{21}\text{Ne}$   
exposure times calculated in Miocene cherts are generally shorter (range between  $0_{-0}^{+59}$  and  
 $242 \pm 113$  kyr) compared to exposure times calculated in the currently eroding chert nodules

presented here ( $269\pm 49$  and  $378\pm 76$  kyr) and other chert surfaces currently eroding in hyperarid  
25 environments. Shorter exposure times in Miocene cherts correspond to faster paleo-erosion rates,  
which we attribute to a combination of continuous surface uplift and significantly wetter climatic  
conditions during the early-mid Miocene.

## 1. Introduction

Tectonic and climatic conditions control geomorphological processes through surface uplift, rock  
30 weathering, and sediment generation and transport (e.g., Allen, 2008; Whipple, 2009; Whittaker,  
2012). Fluvial systems and their associated sediment archives respond to and record changes in  
rates of continental uplift and climatic conditions as rates of erosion influence sediment  
production, transport, and storage (e.g., DiBiase and Whipple, 2011; Ferrier et al., 2013; Vance et  
al., 2003). Cosmogenic nuclides, mostly radiogenic  $^{26}\text{Al}$  and  $^{10}\text{Be}$ , have been used extensively to  
35 study weathering and erosion rates in fluvial systems of different scales and at diverse geological  
settings (e.g., Bierman, 1994; von Blanckenburg, 2005). However, the further back in time we go,  
the less information there is about rates of surface shaping processes in fluvial environments (e.g.,  
erosion, transport, and deposition), and the harder it becomes to reconstruct the tectonic and  
climatic conditions that prevailed. This lack of information is mostly due to decreasing  
40 preservation of older sediments in fluvial systems, as these tend to end up either deeply buried at  
depositional basins or recycled by another erosional process (e.g., Anderson et al., 1996; Guralnik  
et al., 2011; Schaller et al., 2002). Furthermore, even when geological circumstances do allow for  
the preservation of older sediments, rates prior to the Pliocene cannot be quantified with the more  
commonly used cosmogenic radionuclides ( $^{10}\text{Be}$  and  $^{26}\text{Al}$ ) due to their half-lives (1.38 Myr and  
45 716 kyr, accordingly; Ivy-Ochs and Kober, 2008). Unlike their radioactive counterparts, stable  
cosmogenic nuclides have the potential to quantify rates of surface processes as far back as Lower  
Cretaceous (Balco et al., 2019; Ben-Israel et al., 2018; Dunai et al., 2005; Libarkin et al., 2002;  
Sinclair et al., 2019). Here, we apply stable cosmogenic  $^{21}\text{Ne}$  to sediments deposited during the  
early-mid Miocene ( $\sim 18$  Ma) by a massive fluvial system that drained parts of the Arabian  
50 Peninsula and Sinai into the Mediterranean prior to the subsidence of the Arava Valley along the  
Dead Sea transform (Garfunkel and Horowitz, 1966; Zilberman and Calvo, 2013). We quantify  
the time of exposure during erosion and transport of Miocene chert pebbles deposited by the

Hazeva River and compare it to exposure times of chert that has been eroding over the recent past (~10<sup>5</sup> yr). Through this comparison, we compare erosion rates during early-mid Miocene to those measured today in hyperarid environments and examine the possible influence of the tectonic and climatic conditions that operated in the region during this time.

## 2. Geological Setting

Following an extended period of transgression that ended in the late Eocene, the Mediterranean Sea retreated to its current location (Garfunkel and Horowitz, 1966). This period of relative tectonic tranquility was followed by a series of tectonic and magmatic events that resulted in the rifting of the Red Sea and the Gulf of Aden in the late Eocene to early Oligocene (~35-30 Ma; e.g., Bohannon et al., 1989; Bosworth et al., 2005; Omar and Steckler, 1995). During the last 20-30 Myr, regional doming associated with the emergence of the Afar plume uplifted the Arabian Peninsula from near sea level to its present elevation of ~1km (e.g., Feinstein et al., 2013; Morag et al., 2019; Wilson et al., 2014). As a result of this uplift, widespread denudation followed, and a regional truncation surface developed in the northern Red Sea and the southern Levant exposing older strata down to Precambrian formations depending on the preexisting structure (Avni et al., 2012). Following these events, during the early-mid Miocene, the uplifted region was drained by a newly established fluvial system, termed the Hazeva River, which flowed northwestward from the eroded terrains towards the Mediterranean Sea, and drained an estimated area >100,000 km<sup>2</sup> (Garfunkel and Horowitz, 1966; Zilberman and Calvo, 2013; Fig. 1). The Hazeva fluvial system operated until the subsidence of the Dead Sea Rift, during the late Miocene to early Pliocene, brought on a dramatic change in morphology, which led to the disruption of this massive fluvial system, the last of its kind in the region (Garfunkel, 1981). By the early Pliocene, the Hazeva River was abandoned, and new independent drainage systems drained the region toward the Dead Sea Basin (Avni et al., 2001).

At present, the mostly clastic sedimentary Miocene sequence deposited by the Hazeva River is preserved mainly in structural lows, karstic systems, and abandoned stream valleys in southern Israel, eastern Sinai, and Jordan (Calvo and Bartov, 2001; Fig. 2). The sediments associated with this Miocene fluvial system comprise the upper section of the Hazeva formation in southern Israel. This formation is divided into two major parts, the lower includes autochthonous conglomerates and lacustrine carbonate units, and the upper part is comprised of allochthonous clastic sequences

typical to fluvial environments (Calvo, 2002). Here we focus on the allochthonous upper part of the Hazeva formation and examine two different silicate members eroded from the uplifted Arabian Plateau and Sinai and deposited simultaneously by the Hazeva River (Zilberman and Calvo, 2013). The first member is sub-rounded monocrystalline quartz-arenite, eroded from Phanerozoic Nubian sandstone, as well as from outcrops of Precambrian crystalline rocks of the Arabian-Nubian shield (Calvo and Bartov, 2001). The second member consists of well-rounded chert pebbles either interbedded with the quartz sand or forming horizons of pebbles in the sandy sequence (Zilberman and Calvo, 2013). The chert comprising these pebbles is sourced only from east of the Dead Sea Rift, and therefore fluvial deposits on the west side containing this "imported chert" (Kolodny, 1965) must have been emplaced prior to rifting. The onset of the Hazeva River is constrained by the Karak dike (~20 Myr) which intrudes the lower section of the Hazeva formation (Calvo and Bartov, 2001). While climatic conditions in the Levant during the Miocene are believed to have been wetter (e.g., Kolodny et al., 2009), currently this region is part of a middle latitude dry warm desert extending from northern Africa to western Asia, with the Negev Desert remaining hyperarid at least since the middle Pleistocene (Amit et al., 2006).

### **3. Methodology and Analytical Procedures**

#### **3.1 Sampling Strategy**

Cosmogenic nuclides in sediments accumulate throughout the sedimentary cycle as near-surface material is exposed during weathering and exposure of the source rock, transport in a specific drainage system, and to a much lesser degree following burial at some intermediate or final destination. Unlike the more commonly used radioactive cosmogenic nuclides, which may decay substantially or even completely over multiple sedimentary cycles,  $^{21}\text{Ne}$  is stable. This means that the concentration of  $^{21}\text{Ne}$  measured in the sediment may have accumulated over several cycles of exposure and deposition, i.e., after the sediment reaches the depositional basin, it can be re-exhumed and once again exposed and transported in a new sedimentary cycle. Therefore, the concentration of cosmogenic  $^{21}\text{Ne}$  measured in sediment represents the total exposure during previous and current sedimentary cycles, unless the sediment is exposed during transport to temperatures exceeding the geological closure temperature of Ne in quartz (90-100°C; Shuster and Farley, 2005). The loss of Ne due to diffusion could occur either during burial at depths of ~2-3 km given a geothermal gradient of 30-50°C/km or if rock temperatures reach high enough

temperatures for an extended time, which has been recorded in hot desert environments (e.g., McFadden et al., 2005).

115 We collected and analyzed ten samples in total. Three samples of quartz sand (MHS1, MHS3, and MHS5), and five individual chert pebbles (MHC2, MHC23, MHC5a MHC2b, and MHC6) were obtained from two Miocene Hazeva exposures (Fig. 2 B-C; Table 1). At both sites, samples were collected from deeply shielded locations to minimize the effects of post-burial production (see section 5.1 for further discussion). The quartz sand and the chert pebbles were both transported by  
120 the Miocene Hazeva system and share an overall similar exposure history. However, the quartz sand was exposed in previous sedimentary cycles throughout the Mesozoic and Paleozoic, where it accumulated cosmogenic  $^{21}\text{Ne}$ . In contrast, the chert was deposited in the Eocene and then exposed, transported, and buried during the Miocene (Avni et al., 2012). Therefore, while the cosmogenic  $^{21}\text{Ne}$  measured in the quartz sand represents multiple sedimentary cycles, the  
125 cosmogenic  $^{21}\text{Ne}$  measured in the chert pebbles represents erosion and transport during a single sedimentary cycle in the Miocene Hazeva River.

Additionally, two individual samples of *in situ* chert nodules (EJC3 and EJC5) were collected from exposed bedrock outcrops of the Eocene source rock in central Jordan (Fig. 2A). Unlike the Miocene samples, which were exposed during at least one full sedimentary cycle, the Jordanian  
130 chert nodules accumulated cosmogenic nuclides only during exhumation to the currently exposed surface. Therefore, the cosmogenic nuclide concentrations measured in the Jordanian cherts represent averaged rates of erosion over the last  $\sim 10^5$  yr.

### 3.2 Preparation of Chert and Quartz Samples and Analytical Procedures

Chert pebbles (ranging 4-14 cm, b axis) were crushed and both chert and sand samples were sieved  
135 to 250-850  $\mu\text{m}$ . Chert and quartz samples were processed to separate clean  $\text{SiO}_2$  at the Institute of Earth Sciences Cosmogenic Isotope Laboratory, Hebrew University of Jerusalem, following standard procedures (Hetzl et al., 2002; Kohl and Nishiizumi, 1992). The samples were first leached in  $\text{HCl}/\text{HNO}_3$  mixture (3:1) at a temperature of  $150^\circ\text{C}$  for 1.5h dissolving carbonates and iron oxides. This procedure was followed by Franz magnetic separation to remove magnetic grains,  
140 including quartz grains that contain inclusions of magnetic material. Samples were then leached three times in a 1%  $\text{HF}/\text{HNO}_3$  mixture for 7, 12 and 24h at  $70^\circ\text{C}$ , removing the outer rims of the quartz grains. Aliquots of all ten etched samples were then analyzed for Ne isotopes at the Berkeley Geochronology Center. Chert samples were washed with isopropanol to remove fine chert particles

attached to the chert grains. Aliquots from samples MCH5A and EJC5 were crushed to compare  
145 the degassing results with the uncrushed aliquots. Ca. 70 mg from the chert samples and ca. 150  
mg from the quartz samples were encapsulated in a tantalum packet and heated under vacuum  
using a diode laser micro-furnace at 2-4 heating steps between 450 and 1250°C for 15 minutes at  
each temperature step. Ne isotope measurements used the BGC "Ohio" system and the procedure  
described in Balco et al., (2019). 20-30 grams of leached and clean quartz from three quartz  
150 samples and three chert samples were processed to separate Be and Al oxides following Kohl and  
Nishiizumi (1992) and Bierman and Caffee (2001). These were then analyzed for  $^{10}\text{Be}/^9\text{Be}$  and  
 $^{26}\text{Al}/^{27}\text{Al}$  at the Centre for Accelerator Mass Spectrometry, Lawrence Livermore National  
Laboratory, and calibrated against house standards and blanks.

### 3.3 Cosmogenic Scaling and Correction Factors

155 Exposure and burial times and erosion rates were calculated based on Balco (2007) and scaled  
using time-independent scaling (Stone, 2000) and production mechanisms based on Balco et al.  
(2008), given sea-level high-latitude production rates of 4.96 atoms/g  $\text{SiO}_2$ /year for  $^{10}\text{Be}$ , 30.6  
atoms/g  $\text{SiO}_2$ /year for  $^{26}\text{Al}$  (Balco et al., 2008), and 18.1 atoms/g  $\text{SiO}_2$  year (Borchers et al., 2016;  
Luna et al., 2018).

## 160 4. Results

### 4.1 $^{21}\text{Ne}$ in Quartz Sand and Cherts

For the chert samples, <2% of the total  $^{21}\text{Ne}$  and no more than 1% of the total  $^{20}\text{Ne}$  measured were  
released above 950°C (see the Supplementary Tables S1-4). Therefore subsequent analyses were  
performed at 450, 700, and 950°C heating steps for chert samples and 950 and 1250°C heating  
165 steps for quartz samples (Table 1). Of the total  $^{21}\text{Ne}$  measured, >85% was released at the low-  
temperature steps, below the 950°C step in the chert samples and below the 1250°C step in the  
quartz samples (see Supplementary Tables S1-4). Also, low-temperature  $^{21}\text{Ne}/^{20}\text{Ne}$  and  $^{22}\text{Ne}/^{20}\text{Ne}$   
ratios fall on the spallation line, within analytical uncertainty. Therefore, we conclude that excess  
 $^{21}\text{Ne}$  relative to an atmospheric isotopic  $^{21}\text{Ne}/^{20}\text{Ne}$  ratio of 0.002959 ( $^{21}\text{Ne}_{\text{ex}} = ^{21}\text{Ne}/^{20}\text{Ne}_{\text{measured}} -$   
170  $^{21}\text{Ne}/^{20}\text{Ne}_{\text{air}}$ ) in the low-temperature steps is a good representation for cosmogenic  $^{21}\text{Ne}$  ( $^{21}\text{Ne}_{\text{cos}}$ ;  
see Supplementary Fig. S8-12). While most samples show some increase in the low-temperature  
 $^{21}\text{Ne}_{\text{ex}}$ , sample MHC2 shows no enrichment in  $^{21}\text{Ne}/^{20}\text{Ne}$  ratio and very little enrichment in  
 $^{22}\text{Ne}/^{20}\text{Ne}$  ratio compared to atmospheric composition in the low-temperature steps. In the 950°C

step, there is enrichment compared to atmospheric values. However, as only ~12% of the total  
175  $^{21}\text{Ne}$  was released in the 950°C step, determining the concentration of cosmogenic  $^{21}\text{Ne}$  in sample  
MHC2 is beyond analytical abilities. Therefore, this sample was not considered in further  
calculations, discussion, and interpretations. It is important to note that even with cosmogenic  
isotopic values of  $^{21}\text{Ne}/^{20}\text{Ne}$  and  $^{22}\text{Ne}/^{20}\text{Ne}$  ratios at the low-temperature steps, distinguishing the  
cosmogenic component of  $^{21}\text{Ne}_{\text{ex}}$  from the nucleogenic component, produced by the decay of U  
180 and Th within the crystal lattice, is not trivial. Nonetheless, as all chert samples (Eocene chert  
nodules and Miocene chert pebbles) share the same lithology, any differences in the  $^{21}\text{Ne}_{\text{ex}}$   
concentrations must be due to the cosmogenic component.

The chert pebbles and quartz sands sampled at both Miocene Hazeva sites show variable  
concentrations of  $^{21}\text{Ne}_{\text{cos}}$  ranging between  $0.00 \pm 1.88 \cdot 10^6$  and  $8.89 \pm 1.83 \cdot 10^6$  atoms/g  $\text{SiO}_2$  (Fig. 3).  
185 At both Miocene Hazeva sites, the cosmogenic  $^{21}\text{Ne}$  concentrations measured in chert pebbles are  
similar or lower compared to sand samples. These measured concentrations agree with our  
understanding that the sand samples contain quartz grains that originated from various sandy units  
that were deposited throughout the Phanerozoic and could have undergone several sedimentary  
cycles before they were exhumed and transported by the Miocene fluvial system. Alternatively,  
190 the sand samples could have higher concentrations of nucleogenic  $^{21}\text{Ne}$  as the source rock for this  
sand is >800 Ma (Kolodner et al., 2009). Conversely, the chert samples are derived from a  
relatively young Eocene source rock and only participated in one sedimentary cycle during the  
Miocene. Both chert nodule samples collected from *in situ* Eocene outcrops show similar  
cosmogenic  $^{21}\text{Ne}$  concentrations, higher compared to the Miocene chert pebbles (Fig 3).

195 Diffusion kinetics of Ne in quartz have been examined experimentally and theoretically (Shuster  
and Farley, 2005; Tremblay et al., 2014) but have yet to be tested on chert samples where it is  
unclear what is the diffusion length-scale of chert crystals. While diffusion kinetics in chert are  
likely to be similar to quartz, more work is needed to determine that with certainty. Nevertheless,  
diffusion is not likely to have been significant over a ~20 Myr timespan in the measured Miocene  
200 chert samples. While temperatures in exposed cherts in the Levant region can reach 60-70°C during  
mid-day in the summertime due to solar heating, it is unlikely that samples that were transported  
fluvially were exposed continuously at the surface. In support of this claim, the examined chert  
samples did not exhibit any visible cracking or fractures commonly identified with thermal

stresses, leading us to believe that temperatures were not high enough to cause significant diffusion  
205 of Ne out of the chert samples.

#### 4.2 $^{10}\text{Be}$ and $^{26}\text{Al}$ in Quartz Sand and Cherts

$^{10}\text{Be}$  and  $^{26}\text{Al}$  concentrations were measured in three Miocene sand samples (MHS1, MHS3, and  
MHS5), the two Eocene chert nodules (EJC3 and EJC5) and two chert pebbles (MHC5b and  
MHC6).  $^{10}\text{Be}$  results for sample MHC5b and  $^{26}\text{Al}$  results for sample MHS1 are not available (Table  
210 1). Miocene sand and chert samples show  $^{10}\text{Be}$  and  $^{26}\text{Al}$  concentrations that are low and consistent  
with extended periods of burial ( $\leq 0.39 \pm 0.03 \cdot 10^5$  atoms/g  $\text{SiO}_2$  for  $^{10}\text{Be}$  and  $\leq 4.33 \pm 0.55 \cdot 10^5$   
atoms/g  $\text{SiO}_2$  for  $^{26}\text{Al}$ ). Currently eroding Eocene nodules show higher concentrations of  $^{10}\text{Be}$  and  
 $^{26}\text{Al}$ , with sample EJC3 showing  $^{26}\text{Al}/^{10}\text{Be}$  ratio that is consistent with production at the surface,  
and sample EJC5 showing a lower  $^{26}\text{Al}/^{10}\text{Be}$  ratio, suggesting a more complicated exposure history  
215 (see Discussion section).

### 5. Discussion

#### 5.1 Correcting for Post-Burial Muonic Produced Cosmogenic $^{21}\text{Ne}$

When examining concentrations of cosmogenic nuclides in sediments that have been buried for  
extended periods, post-burial production needs to be considered. At or near the surface, spallation  
220 interactions are the main pathway for *in situ* production of cosmogenic nuclides accounting for  
>95% for  $^{26}\text{Al}$ ,  $^{10}\text{Be}$ , and  $^{21}\text{Ne}$  (Dunai, 2010). However, the relative contribution of production by  
muon interactions increases with burial depth, and while production rates are relatively low, they  
can be significant when integrated over long periods of time—especially for stable nuclides. The  
post-burial component does not represent surface processes, and therefore, it is crucial to account  
225 for its contribution to the measured cosmogenic component. For radioactive cosmogenic nuclides,  
such as  $^{10}\text{Be}$  and  $^{26}\text{Al}$ , their initial concentrations (acquired during exposure) decrease post burial  
due to radioactive decay, with  $^{26}\text{Al}$  decreasing faster than  $^{10}\text{Be}$  according to their corresponding  
half-lives (e.g., Balco and Rovey, 2008; Granger, 2006; Granger and Muzikar, 2001; Lal, 1991).  
We calculated the expected concentrations of cosmogenic  $^{26}\text{Al}$ ,  $^{10}\text{Be}$ , and  $^{21}\text{Ne}$  in sediments over  
230 a burial period of 18 Myr, the likely age of the fluvial system stabilization (Bar and Zilberman,  
2016). We then compared these calculated concentrations to the measured concentrations of  $^{26}\text{Al}$ ,  
 $^{10}\text{Be}$ , and  $^{21}\text{Ne}_{\text{cos}}$  in Miocene chert and sand samples (Fig. 4). Both  $^{10}\text{Be}$  and  $^{26}\text{Al}$  measurements  
are only available for two buried sand samples, one buried chert pebble, and two *in situ* chert



nodules (Table 1). The measured  $^{10}\text{Be}$  and  $^{26}\text{Al}$  concentrations have reached an equilibrium that is  
235 consistent with an extended period of burial at depths between 20-120 m (given that overburden  
consists of clastic sediments with a density of  $\sim 2 \text{ g/cm}^3$ ). The discrepancy between the current  
burial depth, only tens of meters below the surface, and the deduced burial depth is likely the result  
of surface erosion that occurred during the last  $\sim 2$  Myr (Matmon and Zilberman, 2017 and  
references therein). Additionally, the relatively large uncertainty on muogenic production rates  
240 could account for some of this discrepancy (Balco, 2017; Balco et al., 2019). Our calculations  
show that the cosmogenic  $^{21}\text{Ne}$  produced post-burial over 18 Myr at depths between 20-120 m is  
lower than the  $^{21}\text{Ne}_{\text{ex}}$  measured in the presented samples (including their uncertainties). The  
maximal calculated post-burial cosmogenic  $^{21}\text{Ne}$  concentration accounts for  $\sim 1.3 \cdot 10^6$  atoms/g  
 $\text{SiO}_2$ , which is lower than the analytical uncertainty for all measured Miocene samples except for  
245 MHC2, where no cosmogenic  $^{21}\text{Ne}$  was measured. However, sample MHC2 is not considered in  
the interpretations of the results. Therefore, we consider post-burial cosmogenic  $^{21}\text{Ne}$  production  
to be insignificant for the presented Miocene exposure times.

## 5.2 Calculating Modern and Miocene Exposure Times

Exposure times calculated for exposure at the surface from cosmogenic  $^{21}\text{Ne}$  concentrations  
250 measured in exposed *in situ* chert nodules from the Jordanian Central Plateau (EJC3 and EJC5)  
range between a minimum of 193 kyr and a maximum of 454 kyr (correlating to cosmogenic  $^{21}\text{Ne}$   
concentrations of  $8.08 \pm 1.48 \cdot 10^6$  and  $12.10 \pm 2.43 \cdot 10^6$  atoms/g  $\text{SiO}_2$ ).

In comparison to the Jordanian samples, quantifying how long were samples exposed during the  
Miocene using cosmogenic  $^{21}\text{Ne}$  concentrations is not trivial, most notably due to the challenge in  
255 evaluating the local cosmogenic production rates. The production rate of cosmogenic nuclides  
increases with altitude as the air pressure and shielding effect of the atmosphere decreases (Stone,  
2000). While the latitude of the Arabian Peninsula during the early Miocene was similar to today  
(Meulenkamp and Sissingh, 2003 and references therein), accounting for the elevation of the  
Miocene samples during production of cosmogenic  $^{21}\text{Ne}$  raises two difficulties. Firstly, it is not  
260 possible to determine with certainty the elevation of the Jordanian Central Plateau during the  
Miocene. It is clear that from the Late Cretaceous up until the late Eocene, the Arabian Peninsula  
was mostly submerged below sea level and that during the Oligocene it was uplifted to a sufficient  
elevation to allow for significant surface erosion (Garfunkel, 1988). During the early Miocene,  
broad valleys (500-1000 m wide and  $\sim 100$  m deep) incised the regional truncation surface that

265 developed in the region, where the Hazeva formation was later deposited (Avni et al., 2012). This  
timeline of events lead us to believe that significant surface uplift occurred prior to the initiation  
of the Miocene Hazeva fluvial system at ~18 Ma. Nevertheless, this stratigraphic evidence is not  
enough to determine whether the Arabian Peninsula reached its current elevation during the early-  
mid Miocene or whether additional uplift occurred over the past 20 Myr, and if so how significant  
270 was it. Studies that focus on exhumation along the eastern flank of the Dead Sea Rift do not provide  
clear evidence to constrain the timing of surface uplift. Surface uplift histories based on cooling  
ages (Feinstein et al., 2013), and river profiles (Wilson et al., 2014), conclude that during the last  
~30 Myr the western half of the Arabian Peninsula was uplifted to its current elevation. However,  
in a recent work, Morag et al. (2019) offer that uplift and exhumation along the western side of the  
275 Suez Rift flank slowed substantially post ~18 Ma. One more approach to evaluate the paleo-  
elevation of the Central Jordanian Plateau during the early-mid Miocene is to calculate the  
elevation given distance and slope. Based on fact that the Hazeva fluvial system drained westward  
to its base level at the Mediterranean, most likely over a moderate stream gradient, we can use the  
~200 km distance between the Mediterranean coast and the current location of exposed chert  
280 nodules, with a moderate gradient of ~0.5%, to reach an elevation of ~1 km above sea level. Taking  
into consideration the different types of evidence reported we believe it is reasonable to presume  
that the western flank of the Arabian Peninsula reached its current elevation (~1 km) during the  
early-mid Miocene. However, another difficulty in calculating paleo-production rates is unrelated  
to the elevation of the Central Jordanian Plateau during the time the Hazeva River operated. The  
285 question arises whether it is appropriate to use the elevation of the source rock for production rate  
calculations or whether a spatially averaged elevation should be used instead. Without any tangible  
information about the size and steepness of the catchment area of the Hazeva River, we are unable  
to correct for different elevations and production rates throughout the basin. Although separate, at  
their core, both possible lower paleo-elevation and a basin-wide integrated elevation add  
290 uncertainties that decrease the potential paleo-elevation used for scaling of production rates,  
resulting in longer calculated exposure times. Therefore, accounting for all uncertainties, we  
assume an elevation range of 500-1000 meters above sea level, and latitude of 20-30° for the  
calculated Miocene exposure times.

The calculated exposure times of sediments in the Miocene Hazeva fluvial system are variable,  
295 and range between a minimum of  $0_{-0}^{+59} - 0_{-0}^{+86}$  kyr measured in sample MHC5b and a maximum

of  $278\pm 63$  –  $408\pm 63$  kyr measured in sample MHS5 (Table 2). Comparing the two silicate member, concentrations (and exposure times) of the sand samples are overlapping or higher than the chert samples (Fig. 3). This agrees with our understanding that the cosmogenic  $^{21}\text{Ne}$  measured in the Miocene chert pebbles represents the total time of exposure during exhumation from bedrock coupled with transport in the Hazeva River, while the sand samples have undergone previous sedimentary cycles and contain inherited cosmogenic  $^{21}\text{Ne}$ . Therefore, sand samples cannot be used to calculate the time sediment were exposed during transport in the Hazeva fluvial system or to infer erosion rates.

The cosmogenic  $^{21}\text{Ne}$  exposure times calculated from the Jordanian chert samples range  $269\pm 63$  to  $378\pm 76$  kyr. Exposure times calculated from  $^{10}\text{Be}$  and  $^{26}\text{Al}$  concentration measured in sample EJC5 overlap within uncertainty with  $^{21}\text{Ne}$  calculated exposure values (Table 2). In contrast, exposure times calculated from  $^{10}\text{Be}$  and  $^{26}\text{Al}$  concentrations measured in sample EJC3 are much shorter  $\sim 13$ - $16$  kyr, an order of magnitude difference. While we cannot explain this discrepancy, we believe that the representative results are the longer exposure times. Firstly, the  $^{21}\text{Ne}$  calculated exposure time in sample EJC3 agrees with the  $^{21}\text{Ne}$ ,  $^{26}\text{Al}$ , and  $^{10}\text{Be}$  calculated exposure times for sample EJC5. Secondly, the timescales of exposure times measured in cherts in eroding surfaces at hyperarid Negev Desert are similar and range from  $\sim 2\cdot 10^5$  to  $\sim 2\cdot 10^6$  yr (Boroda et al., 2014; Fruchter et al., 2011; Matmon et al., 2009). We conclude that exposure times in modern Jordanian Central Plateau chert nodules range  $\sim 300$ - $400$  kyr. It is important to note that the calculated exposure times in the Jordanian cherts represent only exposure at the surface, and do not include exposure during transport, in contrast to the Miocene chert pebbles.

Lastly, when examining ancient exposure times, we must first consider the time-scales over which cosmogenic nuclides are averaged. The question arises whether the reported exposure times accurately represent the environmental conditions of a certain period (e.g. the early to mid-Miocene) or if the calculated times are the result of episodic oscillation or catastrophic geomorphic events. For currently exposed *in situ* samples reported here, it is a reasonably simple answer. The modern exposure times are relatively long and so they integrate hundreds of thousands of years over which such oscillations or rare catastrophic events would be averaged. As for the Miocene exposure times, samples were collected from two separate sites and from different depths, so it is unlikely that they all represent the exception. We, therefore, consider the range of times obtained from Miocene samples to be a good representation for Miocene surface processes.

### 5.3 Modern and Miocene Erosion Rates and the Influence of Climate and Tectonics

The calculated exposure times of the Jordanian chert samples are equivalent to erosion rates of ~4-12 mm/kyr (Table 2), which is consistent with erosion rates measured in the region (Matmon and Zilberman, 2017 and references therein). Calculation of paleo-erosion rates is not as straightforward, as Miocene samples were sampled post deposition and represent exposure both during erosion from bedrock and transport in the Hazeva River. However, Miocene exposure times are either shorter or overlap within uncertainty with those of the *in situ* Jordanian chert samples. Thus, the actual bedrock erosion rates during the Miocene must have been faster than modern rates mentioned above.

While we cannot determine how much faster were paleo-erosion during the Miocene, any increase in erosion rates in a hyperarid desert must be the consequence of different environmental conditions that prevailed in the region at that time. An increase in rates of erosion is most commonly attributed to perturbations in fluvial basins in response to tectonic uplift and/or warmer/wetter climatic conditions (e.g., DiBiase and Whipple, 2011; Romans et al., 2016; Schaller and Ehlers, 2006; Val et al., 2016; Willenbring et al., 2013). For example, increased precipitation brings about higher river discharge and enhancement of the stream power available for bedrock erosion and sediment transport. Erosion rates in fluvial systems also respond to tectonically induced changes in base level that increase slope steepness and instability, resulting in higher stream power and more sediment readily available for transport. Here we examine evidence from previous studies of the climatic and tectonic conditions that prevailed in the region during the Miocene, capable of forcing the deduced increase in erosion rates.

Many works which quantify the rates and timing of surface uplift related to the rifting of the Red Sea are confined to the edges of the Arabian plate and do not give good constraints for intercontinental uplift (Bar et al., 2016; Morag et al., 2019; Omar et al., 1989; Omar and Steckler, 1995). While some of these studies point to a decrease in exhumation rates during the mid-Miocene (~18 Myr; Morag et al., 2019), surface uplift and topographic changes could still drive large-scale landscape response, manifesting as increased erosion rates and the establishment of the Hazeva fluvial system. Together, the above observations suggest climatic conditions, which could promote erosion rates that are faster than observed rates in hyperarid conditions, and that support the existence of a great and maintained fluvial system, such as the Hazeva River, during the Miocene.

## 6. Conclusions

We compared the cosmogenic  $^{21}\text{Ne}$  measured in chert pebbles and quartz sand eroded and transported during the mid-Miocene (~18 Myr) by the Hazeva River with the chert source rock  
360 (Eocene chert nodules) currently eroding in the Central Jordanian Plateau.

In addition to tectonic forcing, there is ample evidence for a warmer and wetter climate in the region during the Miocene. Locally, the appearance of mammals in the Negev along with arboreal and grassy vegetation during the early-mid Miocene supports a humid environment (Goldsmith et al., 1988; Horowitz, 2002; Tchernov et al., 1987). Tropical to subtropical climate prevailed in the  
365 eastern Arabian Peninsula, as indicated by fossilized mangrove roots (Whybrow and McClure, 1980). Locally, Kolodny et al. (2009), interpreted the  $^{18}\text{O}$  in lacustrine limestone from the lower part of the Hazeva unit to be deposited by  $^{18}\text{O}$ -depleted paleo-meteoric water. They proposed that the presence of a warm ocean to the southeast of the region during the Late Oligocene-Early Miocene resulted in tropical cyclones being more prevalent and increasing rainfall in the region.

We successfully established a novel application for measuring cosmogenic  $^{21}\text{Ne}$  in modern and  
370 Miocene chert samples, expanding the opportunities and settings in which stable cosmogenic nuclides analysis could be used as a tool to quantify geomorphic processes and ascertaining chert as a viable lithologic target for cosmogenic Ne analysis. In modern samples, measurements of cosmogenic nuclides  $^{10}\text{Be}$  and  $^{26}\text{Al}$  generally agree with  $^{21}\text{Ne}$  results. In the Miocene samples, cosmogenic  $^{21}\text{Ne}$  in quartz sand samples is equal or higher compared to Miocene chert pebbles,  
375 agreeing with the geologic understanding that sand has experienced several sedimentary cycles where  $^{21}\text{Ne}$  was produced, while chert experienced only one such cycle in the Miocene Hazeva fluvial system.

Exposure times calculated from the measured cosmogenic  $^{21}\text{Ne}$  concentrations in the Miocene  
380 chert pebbles are shorter compared to the chert nodules currently eroding in the Central Jordanian Plateau. While, it is impossible to determine the exact rate of erosion during the Miocene, as cosmogenic  $^{21}\text{Ne}$  was produced during erosion from the bedrock and transport in the river, shorter exposure times during the Miocene point to rates of surface erosion being faster. The cause for increased rates during the early-mid Miocene cannot be easily constrained to either tectonic or  
385 climatic conditions. The entire region experienced tectonic uplift and exhumation that while possibly decreasing during the mid-Miocene, brought on topographic changes that established the Hazeva fluvial system and could have manifested as faster rates of surface erosion. In addition,

multiple independent proxies presented in previous studies support wetter climatic conditions in the region during the early-mid Miocene. Increased precipitation would explain the faster rates of bedrock erosion deduced as well as the higher water discharge needed to maintain transport along the Hazeva River. Finally, the variability observed in exposure times of Miocene chert pebbles might represent a change in rates of erosion throughout the Miocene. However, this variability in  $^{21}\text{Ne}$  concentrations is more likely the result of fluvial transport dynamics, temporary storage, and exposure during transport in this large Miocene river.

### 395 **Data availability**

A raw data table including all Ne isotope measurements and three-isotope plots are available in supplement.

### **Author contribution**

MBI and AM designed the study. MBI collected the samples for analysis with assistance from AM and YA. MBI prepared samples for analyses and measured  $^{21}\text{Ne}/^{20}\text{Ne}$  and  $^{22}\text{Ne}/^{20}\text{Ne}$  ratios with GB, and AJH measured the  $^{10}\text{Be}/^9\text{Be}$  and  $^{26}\text{Al}/^{27}\text{Al}$  ratios. MBI analyzed the data, produced the figures, and prepared the manuscript with contributions from all co-authors.

### **Competing interests**

The authors declare that they have no conflict of interest.

### 405 **Acknowledgments**

This work was funded by the Israel Science Foundation (*ISF* grant number 385/14 to AM) and further supported by the United States-Israel Binational Science Foundation (BSF travel grant T-2017229 to MBI). We greatly appreciate the intensive work and insightful comments by Prof. Taylor Schildgen, Dr. Marissa Tremblay, and an anonymous reviewer. Our gratitude to Y. Geller, O. Tirosh, and Y. Burstyn for laboratory and field assistance. MBI would like to thank the technical and administrative staff at the Berkeley Geochronology Center for their assistance and support. This work was performed in part under the auspices of the U.S. Department of Energy by Lawrence

Livermore National Laboratory, United States under Contract [DE-AC52-07NA27344](#). This is LLNL-JRNL-788357.

415 **References**

Allen, P. A.: From landscapes into geological history, *Nature*, 451(7176), 274–276, doi:10.1038/nature06586, 2008.

Anderson, R. S., Repka, J. L. and Dick, G. S.: Explicit treatment of inheritance in dating depositional surfaces using in situ  $^{10}\text{Be}$  and  $^{26}\text{Al}$ , *Geology*, 24(1), 47, doi:10.1130/0091-7613(1996)024<0047:ETOIID>2.3.CO;2, 1996.

Avni, Y., Bartov, Y., Ginat, H. and Ginata, H.: The Arava Formation-A Pliocene sequence in the Arava Valley and its western margin, southern Israel, *Isr. J. Earth Sci.*, 50(2), 101–120, doi:10.1092/5U6A-RM5E-M8E3-QXM7, 2001.

Avni, Y., Segev, A. and Ginat, H.: Oligocene regional denudation of the northern Afar dome: Pre- and syn-breakup stages of the Afro-Arabian plate, *Bull. Geol. Soc. Am.*, 124(11–12), 1871–1897, doi:10.1130/B30634.1, 2012.

Balco, G.: Production rate calculations for cosmic-ray-muon-produced  $^{10}\text{Be}$  and  $^{26}\text{Al}$  benchmarked against geological calibration data, *Quat. Geochronol.*, 39, 150–173, doi:10.1016/j.quageo.2017.02.001, 2017.

430 Balco, G. and Rovey, C. W.: An isochron method for cosmogenic-nuclide dating of buried soils and sediments, *Am. J. Sci.*, 308(10), 1083–1114, doi:10.2475/10.2008.02, 2008.

Balco, G., Blard, P.-H., Shuster, D. L., Stone, J. O. H. and Zimmermann, L.: Cosmogenic and nucleogenic  $^{21}\text{Ne}$  in quartz in a 28-meter sandstone core from the McMurdo Dry Valleys, Antarctica, *Quat. Geochronol.*, 52, 63–76, doi:10.1016/j.quageo.2019.02.006, 2019.

435 Bar, O. and Zilberman, E.: Subsidence and conversion of the Dead Sea basin to an inland erosion base level in the early middle Miocene as inferred from geomorphological analysis of its ancient western fluvial outlet, *Geomorphology*, 261, 147–161, doi:10.1016/j.geomorph.2016.02.028, 2016.

440 Bar, O., Zilberman, E., Feinstein, S., Calvo, R. and Gvirtzman, Z.: The uplift history of the Arabian Plateau as inferred from geomorphologic analysis of its northwestern edge, *Tectonophysics*, 671, 9–23, doi:10.1016/j.tecto.2016.01.004, 2016.

Ben-Israel, M., Matmon, A., Haviv, I. and Niedermann, S.: Applying stable cosmogenic  $^{21}\text{Ne}$  to

- understand surface processes in deep geological time ( $10^7$ – $10^8$ yr), *Earth Planet. Sci. Lett.*, 498, 266–274, doi:10.1016/j.epsl.2018.07.002, 2018.
- 445 Bierman, P. R.: Using in situ produced cosmogenic isotopes to estimate rates of landscape evolution: A review from the geomorphic perspective, *J. Geophys. Res.*, 99(B7), 13885–13896, doi:10.1029/94JB00459, 1994.
- Bierman, P. R. and Caffee, M.: Slow Rates of Rock Surface Erosion and Sediment Production across the Namib Desert and Escarpment, Southern Africa, *Am. J. Sci.*, 301(4–5), 326–358, 450 doi:10.2475/ajs.301.4-5.326, 2001.
- von Blanckenburg, F.: The control mechanisms of erosion and weathering at basin scale from cosmogenic nuclides in river sediment, *Earth Planet. Sci. Lett.*, 237(3–4), 462–479, doi:10.1016/j.epsl.2005.06.030, 2005.
- Bohannon, R. G., Naeser, C. W., Schmidt, D. L. and Zimmermann, R. A.: The timing of uplift, 455 volcanism, and rifting peripheral to the Red Sea: A case for passive rifting?, *J. Geophys. Res.*, 94(B2), 1683, doi:10.1029/JB094iB02p01683, 1989.
- Borchers, B., Marrero, S., Balco, G., Caffee, M., Goehring, B., Lifton, N., Nishiizumi, K., Phillips, F., Schaefer, J. and Stone, J.: Geological calibration of spallation production rates in the CRONUS-Earth project, *Quat. Geochronol.*, 31, 188–198, doi:10.1016/j.quageo.2015.01.009, 460 2016.
- Boroda, R., Matmon, A., Amit, R., Haviv, I., Arnold, M., Aumaître, G., Bourlès, D. L., Keddadouche, K., Eyal, Y. and Enzel, Y.: Evolution and degradation of flat-top mesas in the hyper-arid Negev, Israel revealed from  $^{10}\text{Be}$  cosmogenic nuclides, *Earth Surf. Process. Landforms*, 1621, 1611–1621, doi:10.1002/esp.3551, 2014.
- 465 Bosworth, W., Huchon, P. and McClay, K.: The Red Sea and Gulf of Aden Basins, *J. African Earth Sci.*, 43(1–3), 334–378, doi:10.1016/j.jafrearsci.2005.07.020, 2005.
- Calvo, R.: Stratigraphy and petrology of the Hazeva Formation in the Arava and the Negev: Implications for the development of sedimentary basins and the morphotectonics of the Dead Sea Rift Valley, *Geol. Surv. Isr. Rep.*, GSI/22/02, 1–264, doi:GSI/22/02, 2002.
- 470 Calvo, R. and Bartov, Y.: Hazeva Group, southern Israel: New observations, and their implications for its stratigraphy, paleogeography, and tectonics, *Isr. J. Earth Sci.*, 50, 71–99, doi:10.1560/B02L-6K04-UFQL-KUE3, 2001.
- DiBiase, R. A. and Whipple, K. X.: The influence of erosion thresholds and runoff variability on



- the relationships among topography, climate, and erosion rate, *J. Geophys. Res.*, 116(F4),  
475 F04036, doi:10.1029/2011JF002095, 2011.
- Dunai, T. J.: *Cosmogenic Nuclides: Principles, Concepts and Applications in the Earth Surface Sciences*, edited by Intergovernmental Panel on Climate Change, Cambridge University Press, Cambridge., 2010.
- Dunai, T. J., González López, G. a. and Juez-Larré, J.: Oligocene-Miocene age of aridity in the  
480 Atacama Desert revealed by exposure dating of erosion-sensitive landforms, *Geology*, 33(4),  
321–324, doi:10.1130/G21184.1, 2005.
- Feinstein, S., Eyal, M., Kohn, B. P., Steckler, M. S., Ibrahim, K. M., Moh'd, B. K. and Tian, Y.:  
Uplift and denudation history of the eastern Dead Sea rift flank, SW Jordan: Evidence from  
apatite fission track thermochronometry, *Tectonics*, 32(5), 1513–1528, 2013.
- 485 Ferrier, K. L., Huppert, K. L. and Perron, J. T.: Climatic control of bedrock river incision,  
*Nature*, 496(7444), 206–209, doi:10.1038/nature11982, 2013.
- Fruchter, N., Matmon, A., Avni, Y. and Fink, D.: Revealing sediment sources, mixing, and  
transport during erosional crater evolution in the hyperarid Negev Desert, Israel,  
*Geomorphology*, 134(3–4), 363–377, doi:10.1016/J.GEOMORPH.2011.07.011, 2011.
- 490 Garfunkel, Z.: Internal structure of the Dead Sea leaky transform (rift) in relation to plate  
kinematics, *Tectonophysics*, 80, 81–108, doi:10.1016/0040-1951(81)90143-8, 1981.
- Garfunkel, Z. and Horowitz, A.: The upper Tertiary and Quaternary morphology of the Negev,  
Israel, *Isr. J. Earth Sci.*, 15(3), 101–117, 1966.
- Goldsmith, N. F., Hirsch, F., Friedman, G. M., Tchernov, E., Derin, B., Gerry, E., Horowitz, A.  
495 and Weinberger, G.: Rotem mammals and Yeroham crassostreids: stratigraphy of the Hazeva  
Formation (Israel) and the paleogeography of Miocene Africa, *Newsletters Stratigr.*, 20(2), 73–  
90, 1988.
- Granger, D. E.: A review of burial dating methods using  $^{26}\text{Al}$  and  $^{10}\text{Be}$ , in *Special Paper 415: In  
Situ-Produced Cosmogenic Nuclides and Quantification of Geological Processes*, vol. 415,  
500 edited by A. M. Alonso-Zarza and L. H. Tanner, pp. 1–16, Geological Society of America.,  
2006.
- Granger, D. E. and Muzikar, P. F.: Dating sediment burial with in situ-produced cosmogenic  
nuclides: theory, techniques, and limitations, *Earth Planet. Sci. Lett.*, 188(1–2), 269–281,  
doi:10.1016/S0012-821X(01)00309-0, 2001.

- 505 Guralnik, B., Matmon, A., Avni, Y., Porat, N. and Fink, D.: Constraining the evolution of river terraces with integrated OSL and cosmogenic nuclide data, *Quat. Geochronol.*, 6(1), 22–32, doi:10.1016/J.QUAGEO.2010.06.002, 2011.
- Hetzl, R., Niedermann, S., Ivy-Ochs, S., Kubik, P. W., Tao, M. and Gao, B.:  $^{21}\text{Ne}$  versus  $^{10}\text{Be}$  and  $^{26}\text{Al}$  exposure ages of fluvial terraces: the influence of crustal Ne in quartz, *Earth Planet. Sci. Lett.*, 201(3–4), 575–591, doi:10.1016/S0012-821X(02)00748-3, 2002.
- 510 Horowitz, A.: Elephants, horses, humans, and others: Paleoenvironments of the Levantine land bridge, *Isr. J. Earth Sci.*, 51(3–4), 203–209, doi:10.1560/YTDR-LW6B-VHR7-69PY, 2002.
- Ivy-Ochs, S. and Kober, F.: Surface exposure dating with cosmogenic nuclides, *Quat. Sci. J.*, 57, 179–209, doi:10.3285/eg.57.1-2.7, 2008.
- 515 Kohl, C. P. and Nishiizumi, K.: Chemical isolation of quartz for measurement of in-situ - produced cosmogenic nuclides, *Geochim. Cosmochim. Acta*, 56(9), 3583–3587, doi:10.1016/0016-7037(92)90401-4, 1992.
- Kolodner, K., Avigad, D., Ireland, T. R. and Garfunkel, Z.: Origin of lower cretaceous ('Nubian') sandstones of North-east Africa and arabia from detrital zircon U-Pb SHRIMP dating, *Sedimentology*, 56(7), 2010–2023, doi:10.1111/j.1365-3091.2009.01067.x, 2009.
- 520 Kolodny, Y.: The lithostratigraphy and petrology of the Mishash chert Formation, The Hebrew University, Jerusalem., 1965.
- Kolodny, Y., Calvo, R. and Rosenfeld, D.: “Too low”  $\delta^{18}\text{O}$  of paleo-meteoric, low latitude, water; do paleo-tropical cyclones explain it?, *Palaeogeogr. Palaeoclimatol. Palaeoecol.*, 280(3–4), 387–395, doi:10.1016/j.palaeo.2009.06.025, 2009.
- 525 Lal, D.: Cosmic ray labeling of erosion surfaces: in situ nuclide production rates and erosion models, *Earth Planet. Sci. Lett.*, 104(2–4), 424–439, doi:10.1016/0012-821X(91)90220-C, 1991.
- Libarkin, J. C., Quade, J., Chase, C. G., Poets, J. and McIntosh, W.: Measurement of ancient cosmogenic  $^{21}\text{Ne}$  in quartz from the 28 Ma Fish Canyon Tuff, Colorado, *Chem. Geol.*, 186, 199–213, doi:10.1016/S0009-2541(01)00411-9, 2002.
- 530 Luna, L. V., Bookhagen, B., Niedermann, S., Rugel, G., Scharf, A. and Merchel, S.: Glacial chronology and production rate cross-calibration of five cosmogenic nuclide and mineral systems from the southern Central Andean Plateau, *Earth Planet. Sci. Lett.*, 500, 242–253, doi:10.1016/j.epsl.2018.07.034, 2018.
- 535 Matmon, A. and Zilberman, E.: Landscape Evolution along the Dead Sea Fault and its Margins,

- in Quaternary of the Levant, edited by Y. Enzel and O. Bar-Yosef, pp. 17–30, Cambridge University Press., 2017.
- Matmon, A., Simhai, O., Amit, R., Haviv, I., Porat, N., McDonald, E., Benedetti, L. and Finkel, R.: Desert pavement-coated surfaces in extreme deserts present the longest-lived landforms on Earth, *Geol. Soc. Am. Bull.*, 121(5–6), 688–697, doi:10.1130/B26422.1, 2009.
- McFadden, L. D., Eppes, M. C., Gillespie, A. R. and Hallet, B.: Physical weathering in arid landscapes due to diurnal variation in the direction of solar heating, *Geol. Soc. Am. Bull.*, 117(1–2), 161–173, 2005.
- Meulenkamp, J. E. and Sissingh, W.: Tertiary palaeogeography and tectonostratigraphic evolution of the Northern and Southern Peri-Tethys platforms and the intermediate domains of the African–Eurasian convergent plate boundary zone, *Palaeogeogr. Palaeoclimatol. Palaeoecol.*, 196(1–2), 209–228, doi:10.1016/S0031-0182(03)00319-5, 2003.
- Morag, N., Haviv, I., Eyal, M., Kohn, B. P. and Feinstein, S.: Early flank uplift along the Suez Rift: Implications for the role of mantle plumes and the onset of the Dead Sea Transform, *Earth Planet. Sci. Lett.*, 516, 56–65, doi:10.1016/j.epsl.2019.03.002, 2019.
- Omar, G. I. and Steckler, M. S.: Fission Track Evidence on the Initial Rifting of the Red Sea: Two Pulses, No Propagation, *Science (80-. )*, 270(5240), 1341–1344, doi:10.1126/science.270.5240.1341, 1995.
- Omar, G. I., Steckler, M. S., Buck, W. R. and Kohn, B. P.: Fission-track analysis of basement apatites at the western margin of the Gulf of Suez rift, Egypt: evidence for synchronicity of uplift and subsidence, *Earth Planet. Sci. Lett.*, 94(3–4), 316–328, doi:10.1016/0012-821X(89)90149-0, 1989.
- Romans, B. W., Castelltort, S., Covault, J. A., Fildani, A. and Walsh, J. P.: Environmental signal propagation in sedimentary systems across timescales, *Earth-Science Rev.*, 153, 7–29, doi:10.1016/j.earscirev.2015.07.012, 2016.
- Schaller, M. and Ehlers, T. A.: Limits to quantifying climate driven changes in denudation rates with cosmogenic radionuclides, *Earth Planet. Sci. Lett.*, 248(1–2), 153–167, doi:10.1016/j.epsl.2006.05.027, 2006.
- Schaller, M., Von Blanckenburg, F., Veldkamp, A., Tebbens, L. A., Hovius, N. and Kubik, P. W.: A 30 000 yr record of erosion rates from cosmogenic  $^{10}\text{Be}$  in Middle European river terraces, *Earth Planet. Sci. Lett.*, 204(1–2), 307–320, 2002.

- Shuster, D. L. and Farley, K. A.: Diffusion kinetics of proton-induced  $^{21}\text{Ne}$ ,  $^3\text{He}$ , and  $^4\text{He}$  in quartz, *Geochim. Cosmochim. Acta*, 69(9), 2349–2359, doi:10.1016/j.gca.2004.11.002, 2005.
- 570 Sinclair, H. D., Stuart, F. M., Mudd, S. M., McCann, L. and Tao, Z.: Detrital cosmogenic  $^{21}\text{Ne}$  records decoupling of source-to-sink signals by sediment storage and recycling in Miocene to present rivers of the Great Plains, Nebraska, USA, *Geology*, 47(1), 3–6, doi:10.1130/G45391.1, 2019.
- Tchernov, E., Ginsburg, L., Tassy, P. and Goldsmith, N. F.: Miocene mammals of the Negev (Israel), *J. Vertebr. Paleontol.*, 7(3), 284–310, doi:10.1080/02724634.1987.10011661, 1987.
- 575 Tremblay, M. M., Shuster, D. L. and Balco, G.: Diffusion kinetics of  $^3\text{He}$  and  $^{21}\text{Ne}$  in quartz and implications for cosmogenic noble gas paleothermometry, *Geochim. Cosmochim. Acta*, 142, 186–204, doi:10.1016/j.gca.2014.08.010, 2014.
- Val, P., Hoke, G. D., Fosdick, J. C. and Wittmann, H.: Reconciling tectonic shortening, sedimentation and spatial patterns of erosion from  $^{10}\text{Be}$  paleo-erosion rates in the Argentine Precordillera, *Earth Planet. Sci. Lett.*, 450, 173–185, doi:10.1016/j.epsl.2016.06.015, 2016.
- 580 Vance, D., Bickle, M., Ivy-Ochs, S. and Kubik, P. W.: Erosion and exhumation in the Himalaya from cosmogenic isotope inventories of river sediments, *Earth Planet. Sci. Lett.*, 206(3–4), 273–288, doi:10.1016/S0012-821X(02)01102-0, 2003.
- Whipple, K. X.: The influence of climate on the tectonic evolution of mountain belts, *Nat. Geosci.*, 2(2), 97–104, doi:10.1038/ngeo413, 2009.
- 585 Whittaker, A. C.: How do landscapes record tectonics and climate?, *Lithosphere*, 4(2), 160–164, doi:10.1130/RF.L003.1, 2012.
- Whybrow, P. J. and McClure, H. A.: Fossil mangrove roots and palaeoenvironments of the miocene of the eastern Arabian Peninsula, *Palaeogeogr. Palaeoclimatol. Palaeoecol.*, 32, 213–225, doi:10.1016/0031-0182(80)90041-3, 1980.
- 590 Willenbring, J. K., Gasparini, N. M., Crosby, B. T. and Brocard, G.: What does a mean mean? The temporal evolution of detrital cosmogenic denudation rates in a transient landscape, *Geology*, 41(12), 1215–1218, doi:10.1130/G34746.1, 2013.
- Wilson, J. W. P., Roberts, G. G., Hoggard, M. J. and White, N. J.: Cenozoic epeirogeny of the Arabian Peninsula from drainage modeling, *Geochemistry, Geophys. Geosystems*, 15(10), 3723–3761, doi:10.1002/2014GC005283, 2014.
- 595 Zilberman, E. and Calvo, R.: Remnants of Miocene fluvial sediments in the Negev Desert, Israel,

and the Jordanian Plateau: Evidence for an extensive subsiding basin in the northwestern margins of the Arabian plate, *J. African Earth Sci.*, 82, 33–53,  
600 doi:10.1016/j.jafrearsci.2013.02.006, 2013.

**Table 1: Sample Description, Sampling Site Locations and Cosmogenic Nuclide Data**

Sample	Sample type	Site	Sampling depth below surface (m)	Location		Elevation (m.a.s.l)	Be Carrier (mg)	<sup>10</sup> Be/ <sup>9</sup> Be (×10 <sup>-13</sup> )	[ <sup>10</sup> Be] (10 <sup>5</sup> atoms/g SiO <sub>2</sub> )	<sup>26</sup> Al/ <sup>27</sup> Al	[Al]*	[ <sup>26</sup> Al]	Al/Be	[ <sup>21</sup> Ne <sub>cos</sub> ] <sup>†</sup>
				Lat (°N)	Long (°E)						(ppm)	10 <sup>5</sup> atoms/g SiO <sub>2</sub> )		
MHS1	Quartz sand	Paran Valley, Israel	30	30.33296	34.92724	290	176	0.17±0.03	0.14±0.02	NA	104	NA	NA	MHS1
MHS3	Quartz sand	Arad Quarry, Israel	90	31.23372	35.20685	570	171	0.36±0.02	0.29±0.02	0.60±0.08	110	1.33±0.17	4.57±0.64	MHS3
MHS5	Quartz sand	Arad Quarry, Israel	100	31.23372	35.20685	570	175	0.32±0.02	0.26±0.02	0.35±0.04	114	0.86±0.11	3.25±0.44	MHS5
MHC2	Chert pebble	Paran Valley, Israel	20	30.33296	34.92724	290	NA	NA	NA	NA	NA	NA	NA	MHC2
MHC3	Chert pebble	Arad Quarry, Israel	90	31.23372	35.20685	570	NA	NA	NA	NA	NA	NA	NA	MHC3
MHC5a	Chert pebble	Arad Quarry, Israel	100	31.23372	35.20685	570	NA	NA	NA	NA	NA	NA	NA	MHC5a
MHC5b	Chert pebble	Arad Quarry, Israel	100	31.23372	35.20685	570	172	NA	NA	0.93±0.12	203	4.33±0.55	NA	MHC5b
MHC6	Chert pebble	Paran Valley, Israel	30	30.33296	34.92724	290	170	0.10±0.01	0.39±0.03	0.05±0.02	287	0.32±0.13	0.83±0.35	MHC6
EJC3	In situ chert	Central Jordanian Plateau	Surface	30.97045	36.64469	910	172	0.70±0.03	1.13±0.05	1.50±0.10	230	6.81±0.43	5.11±0.38	EJC3
EJC5	In situ chert	Central Jordanian Plateau	Surface	30.87181	36.52129	1000	178	18.43±0.30	29.75±0.49	11.47±0.25	235	72.96±1.54	2.45±0.07	EJC5

Note: NA – not available. Samples were either not analyzed, or no result was attained.

\*Measurement uncertainties are ~5%.

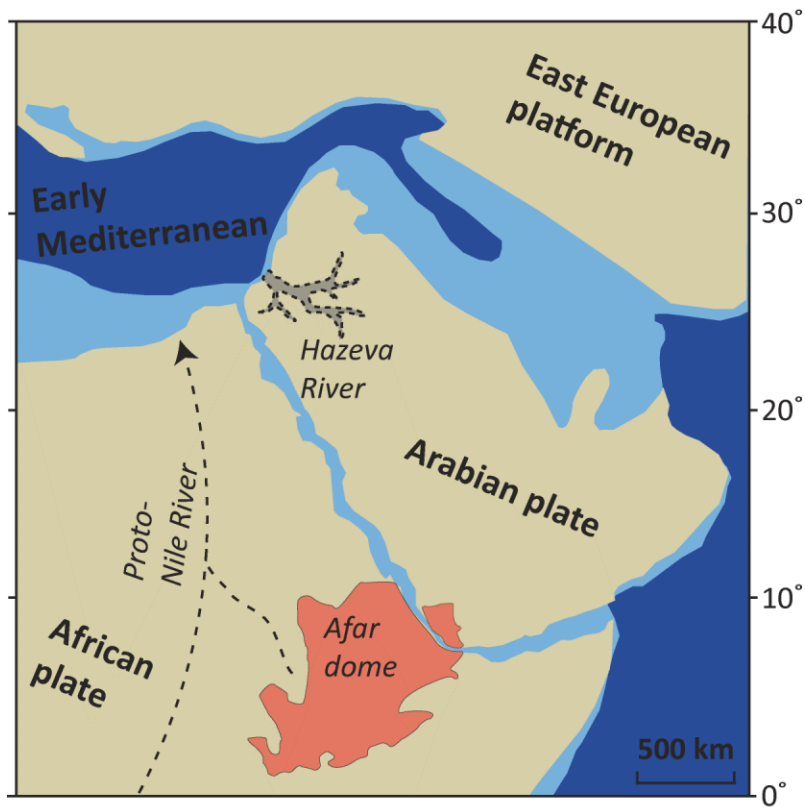
†Cosmogenic <sup>21</sup>Ne is the excess of <sup>21</sup>Ne concentrations relative to the atmospheric <sup>21</sup>Ne/<sup>20</sup>Ne ratio, calculated for the low-temperature steps (<950°C for chert and <1250°C for quartz).

**Table 2: Exposure times and erosion rates calculated for the modern and Miocene samples**

Sample	Sample type	Location	Exposure time (kyr)	Erosion rate (mm/kyr)
MHS1	Miocene quartz sand	Paran Valley, Southern Negev Desert	114±46 – 166±87	-
MHS3	Miocene quartz sand	Arad Quarry, Northeastern Negev Desert	280±10 – 408±63	-
MHS5	Miocene quartz sand	Arad Quarry, Northeastern Negev Desert	278±17 – 404±83	-
MHC3	Miocene chert pebble	Arad Quarry, Northeastern Negev Desert	167±53 – 242±113	3.0±1.4 – 4.4±1.4
MHC5a	Miocene chert pebble	Arad Quarry, Northeastern Negev Desert	91±46 – 132±78	5.5±3.3 – 8.0±4.7
MHC5b	Miocene chert pebble	Arad Quarry, Northeastern Negev Desert	0 <sub>-0</sub> <sup>+59</sup> – 0 <sub>-0</sub> <sup>+85</sup>	>8.6 – >12.4
MHC6	Miocene chert pebble	Paran Valley, Southern Negev Desert	121±59 – 176±102	3.0±1.4 – 4.4±3.5
EJC3*	In situ chert nodule	Central Jordanian Plateau	269±49 / 16±1 / 13±1	2.7±0.5 / 41.7±1.7 / 50.0±3.2
EJC5*	In situ chert nodule	Central Jordanian Plateau	378±76 / 361±6 / 378±3	1.9±0.4 / 1.7±0.0 / 4.4±0.1

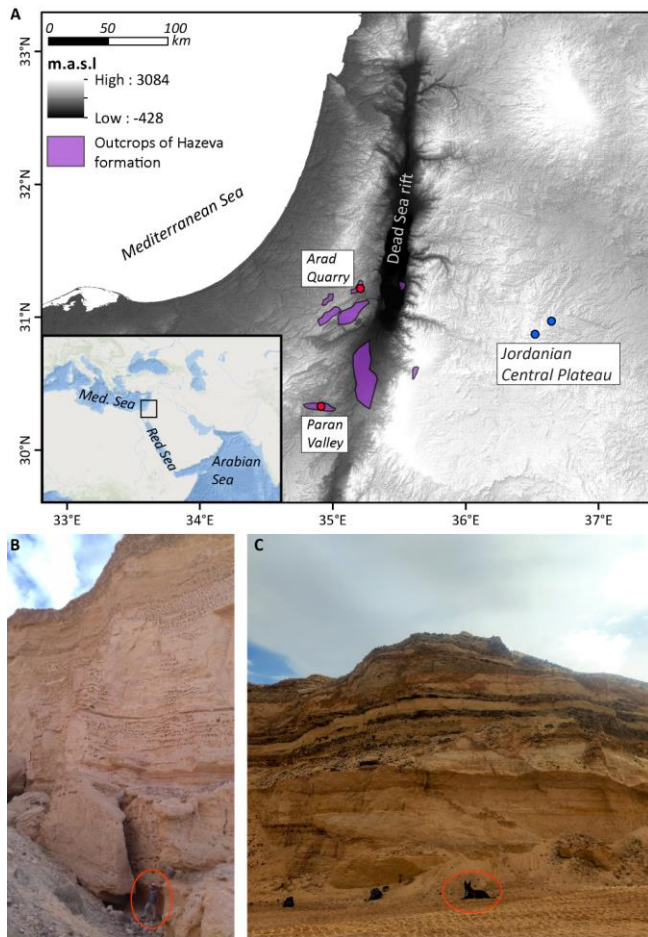
*Note:* Exposure times is the ‘simple exposure time’ calculated for exposure at the surface, calculated cosmogenic <sup>21</sup>Ne production rates ranging 22.2-30 (atoms/g SiO<sub>2</sub> yr), given an elevation of 500 and 1000 meters above sea level. Erosion rates for sand samples were not calculated as the concentration of cosmogenic <sup>21</sup>Ne might include inherited cosmogenic <sup>21</sup>Ne from previous sedimentary cycles.

\*Erosion rates calculated using <sup>21</sup>Ne / <sup>10</sup>Be / <sup>26</sup>Al.



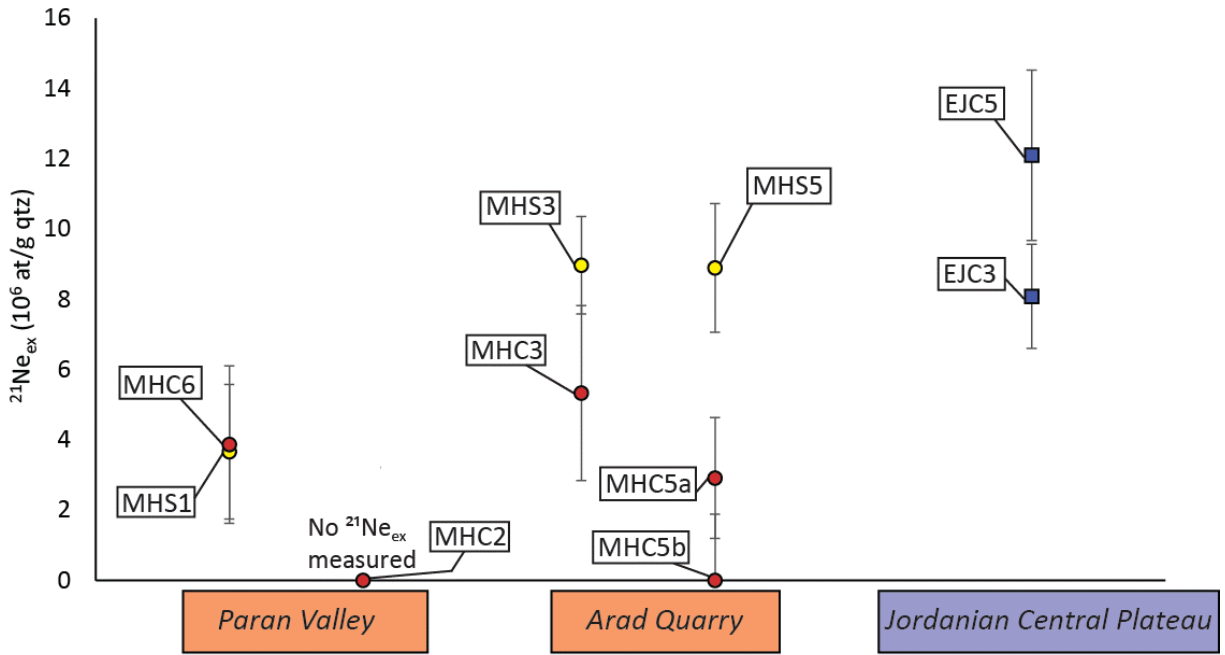
610 **Figure 1. Paleo-geographic map of the eastern Levant during the early Miocene (modified after Meulenkamp and Sissingh, 2003) with the approximated extent of the Hazeva fluvial system (based on Avni et al., 2012; Zilberman and Calvo, 2013).**





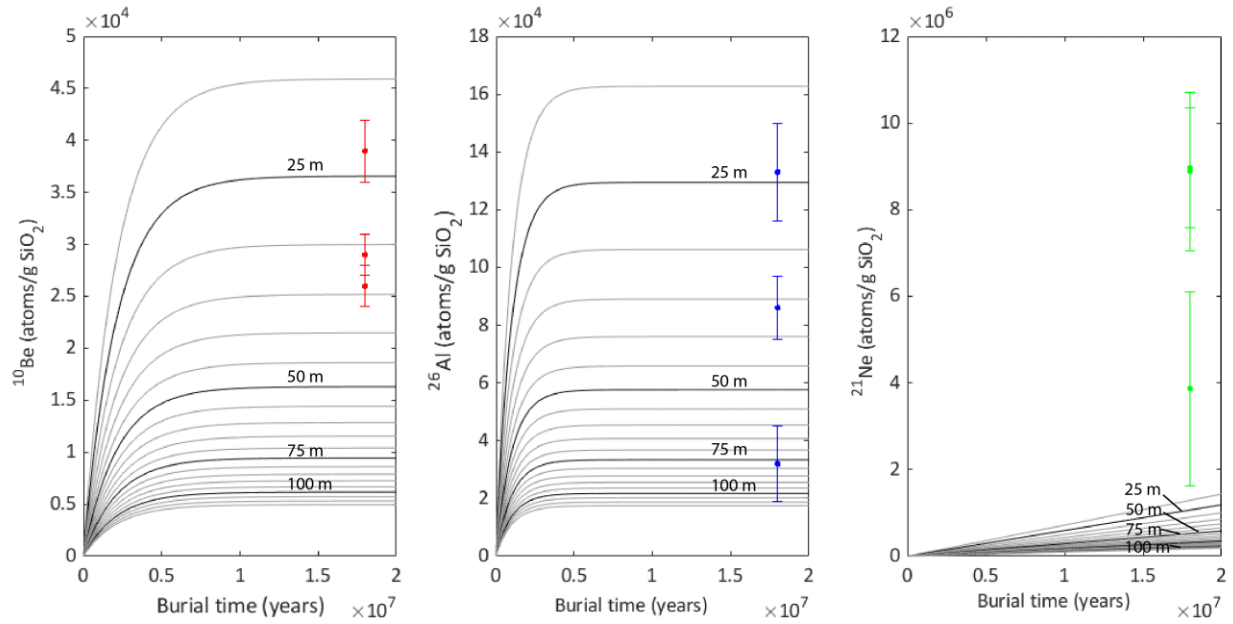
615

**Figure 2. (A) Shaded relief map of the study area with sampling locations of Miocene fluvial sediments sites (red) and in situ Eocene source rock (blue). Hazeva outcrops are after Zilberman and Calvo (2013). Inset map shows regional geographical context. (B) Sampling location at Paran Valley. Sample collected from behind the fallen boulder in a narrow canyon and underneath an overburden of ~50 meters of sand and conglomerate. See person for scale marked at the bottom. (C) Photo of sampling location at Arad Quarry. Samples collected from underneath an overburden of ~100 meters of quartz sand. See dog for scale marked at the bottom.**



620

**Figure 3.**  $^{21}\text{Ne}_{\text{cos}}$  concentrations in Hazeva sands (yellow), Hazeva chert pebbles (red), and *in situ* Jordanian Central Plateau chert nodules (blue) with respective uncertainties.



625 **Figure 4. Measured concentrations of  $^{10}\text{Be}$  (red),  $^{26}\text{Al}$  (blue), and  $^{21}\text{Ne}$  (green) in samples MHS3, MHS5, and MHC6. Grey contour lines show changes in nuclide concentrations with time at different depths from 20 to 120 m below the surface in 5m increments. For both sand samples and chert sample, the concentrations of cosmogenic  $^{21}\text{Ne}$  are higher than the estimated post burial production. Production by cosmic-ray muons is calculated with schematics presented by Balco (2007). Production rates were calculated at the Arad Quarry site by cosmic-ray muons of  $^{10}\text{Be}$  and  $^{26}\text{Al}$  are after Balco (2017) and of  $^{21}\text{Ne}$  by fast muons is after Balco et al. (2019). This shows that  $^{10}\text{Be}$  and  $^{26}\text{Al}$  concentrations can be explained by post-burial production, but  $^{21}\text{Ne}$  concentrations cannot, so a significant fraction of cosmogenic  $^{21}\text{Ne}$  is pre-burial.**

630